Effects of elastic heterogeneity and anisotropy on the morphology of self-assembled epitaxial quantum dots

Chandan Kumar[a] and Lawrence Friedman
Department of Engineering Science and Mechanics, Pennsylvania State University, 212 Earth and Engineering Science Building, University Park, Pennsylvania 16802, USA

(Received 28 February 2008; accepted 30 May 2008; published online 1 August 2008)

Epitaxial self-assembled quantum dots (SAQDs) are of both technological and fundamental interest, but their reliable manufacture still presents a technical challenge. To better understand the formation, morphology, and ordering of epitaxial SAQDs, it is essential to have an accurate model that can aid further experiments and predict the trends in SAQD formation. SAQDs form because of the destabilizing effect of elastic mismatch strain, but most analytic models and some numerical models of SAQD formation either assume an elastically homogeneous anisotropic film-substrate system or assume an elastically heterogeneous isotropic system. In this work, we perform the full film-substrate elastic calculation and incorporate it into a stochastic linear model of the initial stages of SAQD formation process for the case of fast deposition followed by annealing. We find that using homogeneous elasticity can cause errors in the elastic energy density as large as 26%. The wavelength corresponding to the fastest growing mode in the linear model is used as an estimate for SAQD spacing. We calculate that homogeneous elasticity can lead to an error of about 11% in the estimated value of average spacing established during the initial stages of SAQD formation process. We also quantify the effect of elastic heterogeneity on the order estimates of SAQDs and confirm previous finding on the possibility of order enhancement by growing a film near the critical film height. © *2008 American Institute of Physics*. [DOI: 10.1063/1.2960560]

I. INTRODUCTION

Self-assembled quantum dots (SAQDs) function as artificial atoms embedded in a semiconductor matrix.[1] As such, they are useful for a range of electronic and optoelectronic applications.[1–19] For this reason, there has been a great deal of modeling work on their dynamic formation process.[20–41] SAQDs are fabricated by depositing a semiconductor film on a lattice mismatched substrate with a smaller band gap, the most well-known examples being Ge_xSi_{1-x} deposited on Si and $In_xGa_{1-x}As$ deposited on GaAs. A good quantitative model of the SAQD formation can help in aiding understanding of the SAQD formation process and enable a sophisticated quantitative interpretation of experimental data, but more importantly, it can help move modeling from a descriptive mode to a predictive mode that could be used for process design optimization to aid in tasks such as the formation of new structures, control of morphology, and enhancing order and reproducibility.

Many reports in the literature make approximations such as assuming elastic isotropy,[20,35,38,42] elastic homogeneity of the film-substrate system,[24,26,36,37,39,40] or making a thin-film approximation.[22,23] Here, we present a linear stochastic model of the initial stages of SAQD formation process that incorporates anisotropic elasticity and the elastic heterogeneity of the film-substrate system. The order of SAQDs or in other words the placement and spacing of SAQDs is influenced by the order established during the initial stages of SAQD formation process. Here, we investigate the order established during the initial stages (Fig. 1). Furthermore, we investigate the amount of error that previous approximations make (Table I).

While there are other aspects of SAQD modeling that can be improved or incorporated, the presented work is an indispensable step in moving toward a more quantitatively accurate SAQD formation model. The elasticity portion of the calculation applies generally to different material systems, but other parts of the calculation such as surface energies and diffusional dynamics are specific to group IV elements that have fourfold symmetric SAQD formation dynamics such as Ge_xSi_{1-x}/Si,[36,37,43] and not to II-VI systems or III-V systems such as $In_xGa_{1-x}As/GaAs$.

SAQDs result from a transition from two-dimensional film growth to three-dimensional growth in strained epitaxial

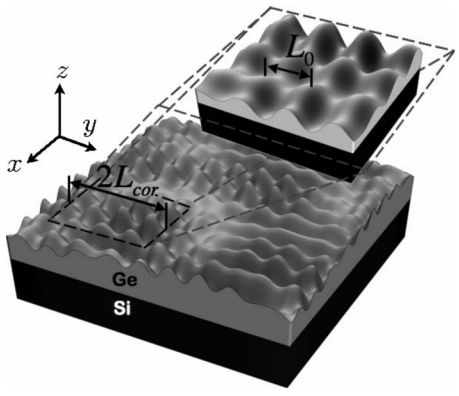

FIG. 1. Initial formation of Ge/Si SAQDs (Sec. II) with exaggerated height fluctuations for clarity. L_0 is mean dot spacing. $2L_{cor}$ is the length over which SAQDs appear periodic. (Sec. III).

[a]Electronic mail: cuk137@psu.edu.

TABLE I. Comparison of presented model with various approximations. Our model uses heterogeneous anisotropic elasticity (Het. Anis.) Other models use homogeneous anisotropic elasticity (Hom. Anis.) (Ref. 24 and 26), anisotropic thin-film elasticity (Anis. Thin), heterogeneous isotropic elasticity (Het. Iso.) (Ref. 21), homogeneous isotropic elasticity (Hom. Iso.), and isotropic thin-film elasticity (Iso. Thin) (Ref. 23). All calculations use average film height $\bar{H}=4.25$ ML and $\mathcal{E}_{0^\circ}(0.154)$ uses $k=2\pi/(49.06\ \text{nm})=0.128\ \text{nm}^{-1}$. Values in parentheses indicate percentage error due to each approximation.

	Het. Anis.	Hom. Anis. (% error)	Anis. Thin (% error)	Het. Iso. (% error)	Hom. Iso. (% error)	Iso. Thin. (% error)
$\mathcal{E}_{0^\circ}(0.154)$	4.18	4.92	3.90	5.64	6.47	5.24
(10^9 ergs/cm^3)		(+18%)	(−7%)	(+35%)	(+56%)	(+25%)
L_E (nm)	55.4	49.2	62.1	39.9	37.4	46.2
		(−11%)	(+12%)	(−28%)	(−32.5%)	(−17%)
L_0 (nm)	49.1	43.7	55.1	35.4	33.2	41.0
		(−11%)	(+12%)	(−28%)	(−32%)	(−17%)
n_{cor}	2.71	2.07	2.62	n/a	n/a	n/a
		(+24%)	(−3%)			

films. When a flat strained film is perturbed by a film height undulation, elastic energy is released. When the released energy is greater than the cost in surface and wetting energy, the perturbation grows. This phenomenon is known as the Asaro–Tiller–Grinfeld instability.[44,45] Eventually the surface perturbations mature into three-dimensional quantum dots. At a later stage the dots ripen,[25,33] although theoretically, they might form a uniform array under some circumstances.[25,29,35,46–49] The interplay of the elastic energy, the surface energy, and the wetting energy determine the energy landscape that drives SAQD formation, and the spectral modeling method used here yields a very transparent description of this interplay.

The spectral model can be used to define and estimate parameters characterizing SAQD formation such as the characteristic length and time scales, the mean SAQD spacing, the alignment of SAQDs in an array, as well as the critical film height for SAQD formation.[20,21,26,37,42,43] In the stochastic form, spectral modeling can also elucidate order and reproducibility of SAQD arrays.[36] In higher order versions of spectral models known as multiscale-multitime analyses, they can even elucidate longer term evolution of SAQDs.[35] The clearly defined parameters from these models also inform finite element based models[30] and provide benchmarking for their performance.

Elasticity is the most well understood influence on SAQD formation. As such, making fewer approximations about elasticity will help investigations into other influences on SAQD formation that are more difficult to understand. For example, wetting energy is barely understood,[30,50,51] and surface energy is generally treated as a constant, even though it almost certainly has strain and temperature dependence. It is also controversial as to whether surfaces should be treated as facets or not.[52,53]

While the importance of getting accurate estimates for a quantity as basic as the mean dot spacing is self-evident, the significance of SAQD order deserves further discussion. The ordering of SAQDs has been a matter of concern in fostering the development of quantum dot based devices.[54] There are two types of order, spatial and size. Spatial order is concerned with the uniformity of the spacings between the SAQDs and size order is concerned with the uniformity in the size of the SAQDs. The size and spacings of these SAQDs are related, as dot volume is limited by the locally available material. Understanding what factors affect the order of SAQDs can guide experiments and simulation efforts and help in interpreting experimental and simulation results. Our enhanced elasticity calculation improves upon recent models of SAQD order.[36,37,43] We defer pattern fidelity in directed self-assembly to later work although some initial results have been previously reported.[38,55]

Previous modeling work has focused on how elastic anisotropy and elastic heterogeneity affect SAQD formation,[22,24,26,35–37,42,56] but the two influences have been treated separately. The effect of elastic anisotropy has been studied in great detail. In Ref. 24 it was shown that for heteroepitaxial system such as $Si_{1-x}Ge_x/Si$, the surface undulations are likely to grow in the ⟨100⟩ directions. It was also shown that for anisotropic materials the growth rate of the amplitude of the surface fluctuations is maximum when the wavelength is 4/3 the cutoff wavelength, similar to the isotropic approximation. However, in the presence of a strong wetting effect, this ratio increases to 2. In the absence of misfit dislocations, the islands are aligned in the ⟨100⟩ directions. However, experiments reveal that for films with thicknesses greater than the critical thickness for dislocation formation, in the later stages of island formation, the islands align along the ⟨110⟩ directions due to the formation of misfit dislocations.[26] In Ref. 56 a numerical investigation was carried out to study the effect of anisotropic strength on the formation, alignment, and average island spacing. More recent analytic studies on SAQD order[36,37,43] complement these numerical studies. The effect of elastic heterogeneity, however, has received more limited attention. In Ref. 42 a linear stability analysis was performed that incorporated the elastic stiffness for both film and the substrate. One major conclusion was that elastically stiff substrate has stabilizing effects on the film that diminishes with increasing film thickness. In Ref. 22 a nonlinear evolution equation was derived using a thin-film approximation. However, Refs. 42 and 22 approximate elasticity as isotropic.

Here, we treat elastic effects without approximations re-

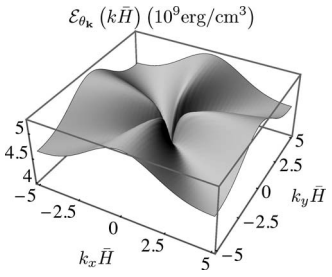

FIG. 2. The elastic energy density prefactor as a function of the dimensionless vector $\mathbf{k}\bar{H}$ for Ge/Si at 600 K.

garding isotropy, homogeneity, or film thickness. We find various parameters that can be derived and estimated from spectral SAQD growth models, and we compare them to the results of the other more approximate models (Table I). These parameters are $\mathcal{E}$, the elastic energy density coefficient (Figs. 2 and 3) that appears in the calculation for elastic energy density [Eq. (3)], L_E, the perturbation wavelength that is the most energetically unstable (Fig. 4), L_0, the perturbation wavelength that is kinetically most unstable and gives the mean dot spacing (Fig. 6), and n_{cor} (Fig. 7) the number of dots in a row whose positions are well correlated. Each of these values is compared to the predictions of more approximate models, namely, the elastically *anisotropic homogeneous* approximation, the elastically anisotropic thin-film approximation, the elastically *isotropic heterogeneous* approximation, the elastically *isotropic homogeneous* approximation, and the elastically *isotropic thin-film* approximation presented recently.[23] For the order analysis, n_{cor}, comparisons are only made with the elastically *anisotropic* models as elastically *isotropic* models are not suitable for order predictions of periodic arrays.[43] Also, all of the reported estimates depend on the average film height ($\bar{H}$); thus for each comparison we present a calculation corresponding to a typical average film height of $\bar{H}$=4.25 ML=1.2 nm in Table I with some additional values displayed in Figs. 3, 4, 6, and 7. It is worth noting that all of these approximations correspond to various limits of our elasticity calculation. For

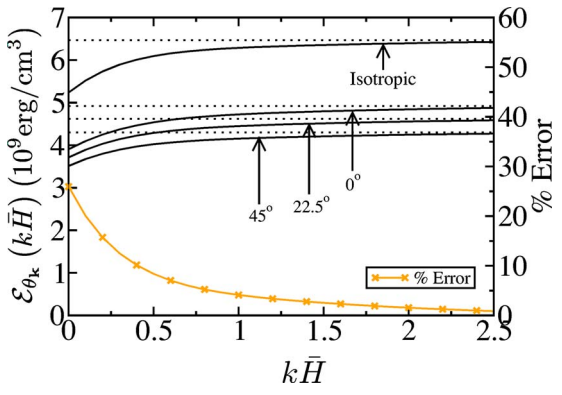

FIG. 3. (Color online) Elastic energy density prefactor $\mathcal{E}_{\theta_k}$ for Ge/Si at 600 K from isotropic approximations (Ref. 42) and anisotropic calculations for $\theta_{\mathbf{k}}$=0°, 22.5°, and 45°. Asymptotically large $\mathbf{k}\bar{H}$ limits corresponds to the anisotropic/isotropic homogeneous approximations and are shown as dotted lines (…). Percent error in the values of $\mathcal{E}_{\theta_k}$ for $\theta_{\mathbf{k}}$=0° is shown for the anisotropic homogeneous approximation.

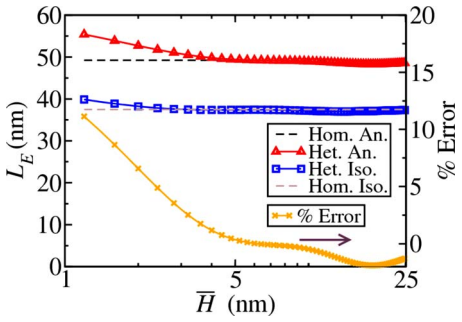

FIG. 4. (Color online) Characteristic wavelength L_E as function of $\bar{H}$ for Ge/Si at 600 K from isotropic and anisotropic calculations. Corresponding homogeneous approximations are shown as dashed lines. The percent error in is shown for the anisotropic homogeneous approximation.

example, the *homogeneous anisotropic* approximation is identical to the limit as the average film height ($\bar{H}$) becomes large. This is reflected in our calculations for $\mathcal{E}$, L_E, L_0, and n_{cor} (Figs. 3, 4, 6, and 7). The *anisotropic thin-film* approximation corresponds to the limit as $\bar{H}\to 0$, and the various isotropic approximations can be obtained by using an isotropic elastic stiffness tensor by, for example, taking the Voigt or Reuss average of the actual elastic moduli. Finally, we give in-depth analysis throughout only for the anisotropic models.

We model the initial stages of SAQD formation process with a stochastic surface diffusion model. We perform a linear analysis of the dynamics of the film evolution, which corresponds to small height fluctuations. Although such an analysis would only be valid for the onset of island formation, it determines the initial placement of SAQDs; thus determining the initial mean spacing (L_0) and order (n_{cor}). At later stages, the SAQDs either order or ripen.[25,34,35,46,56] The spacing and order established at the small fluctuation stage will influence the order at a later stage. This has also been verified through nonlinear calculations in Ref. 36. Linear effects also set the length and the time scale for measuring the perturbations[42] and determine the arrangement of dots. Linearization offers a transparent way for analysis and is also a prerequisite for understanding more advanced nonlinear models. The procedure for order analysis follows Refs. 36, 37, and 43. Most models in literature are deterministic; however, the stochastic model is more realistic, as there is no rigorous physical explanation for the artificial initial random roughness in the deterministic models.

While our elasticity calculations can be used in other models that focus on certain other aspects such as the effects of alloying and compositional variation[57] or stability analysis of a growing film,[42] certain limitations apply to the calculations for estimated dot order because we consider the case of a fast deposition followed by annealing. For many experiments slower deposition rate is of interest. The quantitative values reported here is meant to represent the range of values and the magnitude of errors that could be incurred by not incorporating both elastic heterogeneity and elastic anisotropy in the models for self-assembly of quantum dots.

The rest of this article is organized as follows. We give details of the stochastic surface diffusion model in Sec. II. In

Sec. III we discuss the order calculations using film height correlation functions. We present our conclusions in Sec. IV.

II. MODEL

The formation of SAQDs takes place through surface diffusion that is driven by a diffusion potential μ and contains thermal fluctuations $\boldsymbol{\xi}(\mathbf{x},t)$.[36] μ is a nonlocal functional of the film height H and a function of the horizontal position $\mathbf{x}=(x,y)$ (Fig. 1), so that $\mu \rightarrow \mu[H](\mathbf{x})$.

The normal velocity of the evolving film surface is

$$v_n = D\boldsymbol{\nabla}_s^2 \mu + \boldsymbol{\nabla}_s \cdot \boldsymbol{\xi}(\mathbf{x},t), \tag{1}$$

where $\boldsymbol{\nabla}_s^2$ is the surface laplacian, $\boldsymbol{\nabla}_s \cdot$ is the surface divergence, and we omit explicit coordinate and time dependences for brevity. Here we consider the case of fast deposition followed by annealing of a film and therefore we omit a surface flux term in Eq. (1).

We linearize all quantities about the average film height $\bar{H}$,

$$H(\mathbf{x},t) = \bar{H} + h(\mathbf{x},t), \tag{2}$$

where the average film height $\bar{H}$ can be controlled by controlling the amount of deposited material and $h(\mathbf{x},t)$ represents the fluctuations about this average that cannot be experimentally controlled. In this procedure, the elastic contribution is nonlocal, so analysis is aided by working with Fourier components. We use the convention, $f(\mathbf{x}) = \int d^2\mathbf{x} e^{i\mathbf{k}\cdot\mathbf{x}} f_{\mathbf{k}}$ and $f_{\mathbf{k}} = (2\pi)^{-2} \int d^2\mathbf{k} e^{-i\mathbf{k}\cdot\mathbf{x}} f(\mathbf{x})$. Subscript $\mathbf{k}$ is used to indicate functions of wave vector $\mathbf{k}$, while $(\mathbf{x})$ is used to indicate dependence on the real-space coordinate. We proceed in two steps. First, we linearize the diffusion potential μ. Then, we linearize the dynamic governing equations. Similar to Ref. 37, we keep terms only to linear order in $h(\mathbf{x},t)$.

Previously, the *homogenous* elasticity approximation was used to identify three related wavenumbers and wavelengths,[24,26] the characteristic or cutoff wavenumber and wavelength k_c and $L_c = 2\pi/k_c$ corresponding to the wavenumber above which the modes decay,[21] the wavenumber and wavelength for maximum energy release, $k_E = (1/2)k_c$ and $L_E = 2L_c$,[24,26,35] and the wavenumber and wavelength of the fastest growing mode was identified, k_0 and $L_0 = 2\pi/k_0$.[24,26] For thick films, $k_0 = (3/4)k_c$ $(L_0 = 4/3L_c)$, while for thin films, k_0 ranges from $k_0 = k_E$ $(L_0 = L_E)$ at a critical film height to $k_0 = (4/3)k_E$ $[L_0 = (3/4)L_E]$.[35,37,43] In the less approximate formulation that is elastically *heterogeneous* and *anisotropic*, these relationships are not as simple. In the following analysis, we identify k_E and k_0.

A. Energetics

The diffusion potential μ consists of three parts, $\mu = \mu_{\text{elast.}} + \mu_{\text{surf}} + \mu_{\text{wet.}}$.[22,31,35,43,58] The elastic energy part destabilizes the two-dimensional growth made, the surface energy term stabilizes the short wavelength (high-k) modes, and the wetting potential stabilizes all wavelengths. We proceed by calculating the Fourier transform of the diffusion potential $\mu_{\mathbf{k}}$ to linear order in terms of the Fourier transform of the film height, $h_{\mathbf{k}}$.

1. Elastic anisotropy and heterogeneity

The elastic contribution to the diffusion potential is just the elastic energy density at the film surface, denoted $\omega(\mathbf{x})$ times the atomic volume $[\mu_{\text{elast.}} = \Omega\omega(\mathbf{x})]$.[59] We proceed by calculating the Fourier transform of $\omega(\mathbf{x}), \omega_{\mathbf{k}}$ to linear order in surface height fluctuations $h_{\mathbf{k}}$ while taking into account the effect of both elastic heterogeneity and elastic anisotropy.

The full calculation is described in the Appendix, and it results in an elastic energy density of the form

$$\omega_{\mathbf{k}} = -\mathcal{E}_{\theta_{\mathbf{k}}}(k\bar{H}) k h_{\mathbf{k}}, \tag{3}$$

where $\mathcal{E}_{\theta_{\mathbf{k}}}(k\bar{H})$ is the elastic energy density prefactor that depends on both wave vector direction $\theta_{\mathbf{k}}$ and dimensionless product $k\bar{H}$. This result should be contrasted with previous calculations. In the *homogeneous isotropic* approximation, the prefactor is a constant, and in the homogeneous *anisotropic* approximation, the prefactor depends only on the wavevector direction $\theta_{\mathbf{k}}$.[24,37]

We perform numerical calculations for (001)-oriented Ge/Si at 600 K to give a concrete example of the energy prefactor $\mathcal{E}_{\theta_{\mathbf{k}}}(k\bar{H})$. The elastic stiffness tensor c_{ijkl} is fourfold symmetric for rotations about the [001] axis; thus $\mathcal{E}_{\theta_{\mathbf{k}}}(k\bar{H})$ is also fourfold symmetric. This symmetry manifests itself in the arrangement of SAQDs into a fourfold symmetric quasiperiodic lattice.[24,26,27,37] We use the following physical constants. For Ge at 600 K, the elastic constants are $c_{11}^f = 11.99 \times 10^{11}$ dyn/cm^2, $c_{12}^f = 4.01 \times 10^{11}$ dyn/cm^2, and $c_{44}^f = 6.73 \times 10^{11}$ dyn/cm^2.[60] For Si at 600 K, $c_{11}^s = 15.61 \times 10^{11}$ dyn/cm^2, $c_{12}^s = 5.63 \times 10^{11}$ dyn/cm^2, and $c_{44}^s = 7.82 \times 10^{11}$ dyn/cm^2.[60] Using $a_{\text{Ge}} = 0.5658$ nm and $a_{\text{Si}} = 0.5431$ nm, the mismatch strain is $\epsilon_m = 0.0418$. Figure 2 shows a plot of the elastic energy prefactor $\mathcal{E}_{\theta_{\mathbf{k}}}(k\bar{H})$ against the dimensionless variables $k_x\bar{H}$ and $k_y\bar{H}$. Figure 3 shows $\mathcal{E}_{\theta_{\mathbf{k}}}(k\bar{H})$ as a function of $k\bar{H}$ for three values of $\theta_{\mathbf{k}}$ along with a comparison to the discussed homogenous and isotropic approximations.

Typical values for film height are $\bar{H} < 20$ ML, while typical relevant wavelengths are 30–40 nm; thus, relevant values for $k\bar{H}$ are <1. In Fig. 3, we also plot the error due to the *homogeneous anisotropic* approximation for $\theta_{\mathbf{k}} = 0°$ and $0 \leqslant k\bar{H} \leqslant 2.5$. For values of $k\bar{H} > 2.5$ the error is significantly less (error $<1\%$). It should be noted that we focus primarily on the values at $\theta_{\mathbf{k}} = 0°$ because undulations are more likely to grow in the $\langle 100 \rangle$ directions.[24,26,37] At lower $k\bar{H}$ values $(k\bar{H} < 0.4)$ the error is higher $(>10\%)$ with the upper bound being 26%. For example, for a periodic array of islands spaced at $L_0 = 49.06$ nm $(k = 2\pi/L_0 = 0.128$ nm$^{-1})$ with average film height $\bar{H} = 4.25$ ML $= 1.2$ nm so that $k\bar{H} = 0.154$, the error in the calculation of elastic energy density is about 18%. We find that the *anisotropic thin-film* approximation does a bit better with an error of -7%. We report these final values along with comparisons to other approximations in

Table. I. Such errors limit the accuracy of quantitative models, as this error propagates to calculations of the various characteristic wavenumbers (Secs. II A 3 and II B), mean dot spacing, rate of growth, and critical film height.

2. Surface and wetting energies

The other contributions to the SAQD formation energetics are the surface and wetting energies. Wetting energy is an apparent interaction between the surface of the film and the substrate.[50] Since our focus is on fourfold symmetric systems, the only anisotropic term is due to the elastic energy.[37] As in Ref. 44,

$$\mu_{\mathrm{surf.},\mathbf{k}} = \Omega(\gamma k^2) h_{\mathbf{k}}, \tag{4}$$

where γ can be interpreted as the effective surface energy.[27,37] The linearized wetting potential is

$$\mu_{\mathrm{wet},\mathbf{k}} = \Omega(W'') h_{\mathbf{k}}, \tag{5}$$

where W'' is the second derivative of the wetting potential or the wetting energy density with respect to the film height evaluated at the average film height $H=\bar{H}$. For the example here, we follow Ref. 31 and take the wetting potential to be $W=B/H$, where B is a material constant.

3. Diffusion potential

Combining Eqs. (3)–(5), we can write the fourier transform of the linearized diffusion potential as

$$\mu_{\mathbf{k}} = f(k, \theta_{\mathbf{k}}, \bar{H}) h_{\mathbf{k}}, \tag{6}$$

where $f(k,\theta_{\mathbf{k}},\bar{H}) = \Omega[-k\mathcal{E}_{\theta_{\mathbf{k}}}(k\bar{H}) + \gamma k^2 + W'']$. The minima in $f(k,\theta_{\mathbf{k}},\bar{H})$ lie along the $\langle 100\rangle$ directions ($\theta_{\mathbf{k}}=0°$, 90°, 180°, and 270°) and occur at wavenumber k_E so that the most energy is released when the surface perturbation has a period of $L_E = 2\pi/k_E$. L_E is a function of $\bar{H}$, a dependence that is due purely to the more precise elasticity calculation we present, and not, for example, a result of the wetting potential. For a concrete example, we use the estimated surface energy density $\gamma = 1927$ ergs/cm^2 and the atomic volume $\Omega = 2.27 \times 10^{-23}$ cm^3. Figure 4 shows L_E as a function of $\bar{H}$ along with its values for the *anisotropic homogenous* and isotropic approximations. For an average film height, $\bar{H}=4.25$ ML $=1.2$ nm, the error in L_E from the homogeneous approximation is about 11%. We report results for all approximations in Table I.

The energy cost function is also useful for determining the critical film thickness for SAQD formation, or for modeling purposes it can be used to estimate the wetting potential that leads to an observed critical height. The critical height for SAQD formation in the Ge/Si film-substrate system is generally observed to be 4-6 ML.[61] Here, we choose a critical film height of 4 ML and follow the procedure from Ref. 31. We assume a wetting potential of the form $W(H) = B/H$ and then find the coefficient B that gives a critical film height, $H_c=4$ ML, by setting the minimum value for the energy cost function to zero, $f_{\min} = f(k_E, 0°, H_c) = 0$. Solving for B is a simple procedure as f is linear in B. We find that even the value of B is sensitive to the *anisotropic homogeneous* and other approximations. At 4 ML, $B = 1.61 \times 10^{-6}$ erg/cm for the full theory, and $B = 2.28 \times 10^{-6}$ erg/cm for the *anisotropic homogeneous* approximation, about 42% difference.

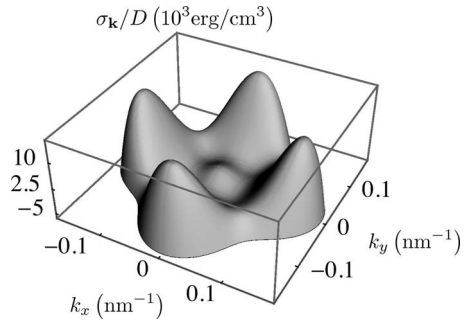

FIG. 5. $\sigma_{\mathbf{k}}/D$ vs $\mathbf{k}$ for $\bar{H}=4.25$ ML for Ge/Si at 600 K.

B. Dispersion relation

The linearized evolution equation in Fourier space is given by[36]

$$\partial_t h_{\mathbf{k}} = \sigma_{\mathbf{k}} h_{\mathbf{k}} + \sqrt{2\Omega D k_b T}[i\mathbf{k}\cdot\boldsymbol{\eta}_{\mathbf{k}}(t)], \tag{7}$$

where the second term is the Fourier transform of $\boldsymbol{\xi}(\mathbf{x},t)$ to linear order, $\langle \boldsymbol{\eta}_{\mathbf{k}}(t)\boldsymbol{\eta}^*_{\mathbf{k}'}(t')\rangle = (2\pi)^{-2}\tilde{I}\delta^2(\mathbf{k}-\mathbf{k}')\delta(t-t')$,[36] and

$$\sigma_{\mathbf{k}} = -Dk^2 f(k, \theta_{\mathbf{k}}, \bar{H}) \tag{8}$$

is the generalized dispersion relation that gives the rate of growth (positive values) or decay (negative values) of each height Fourier component $h_{\mathbf{k}}$.

Figure 5 shows the dispersion relation $\sigma_{\mathbf{k}}$ for $\bar{H}=4.25$ ML. For the case shown in Fig. 5, $\sigma_{\mathbf{k}}$ has four peaks along the $\langle 100\rangle$ directions at $\mathbf{k}_0 = (0, \pm 0.128)$ nm^{-1} and $(\pm 0.128, 0)$ nm^{-1}. The four peaks indicate that the instability is maximum in the $\langle 100\rangle$ directions, thus making them the likely directions for the alignment of SAQDs. This alignment is consistent with previous studies.[24,26,30,37]

Similar to Ref. 37, we expand $\sigma_{\mathbf{k}}$ about its peak values to get

$$\sigma_n = \sigma_0 - \tfrac{1}{2}\sigma_{\parallel}(k-k_{\parallel})^2 - \tfrac{1}{2}\sigma_{\perp}k_{\perp}^2, \tag{9}$$

where

$$\sigma_{\parallel} = -\left.\frac{\partial^2\sigma_{\mathbf{k}}}{\partial k^2}\right|_{[k_0,(\theta_0)_n]}, \quad \sigma_{\perp} = -\frac{1}{k_0^2}\left.\frac{\partial^2\sigma_{\mathbf{k}}}{\partial\theta^2}\right|_{[k_0,(\theta_0)_n]}, \tag{10}$$

n corresponds to the number of peaks, θ_0 is the orientation of $\mathbf{k}_0$, and $k_{\parallel}$ and $k_{\perp}$ are components parallel and perpendicular to $\mathbf{k}_0$. We discuss the dependence of the average dot spacing estimate $L_0 = 2\pi/k_0$ on film thickness next along with the discussion of SAQD array order.

III. ORDER ANALYSIS

The spatial order of SAQDs is best characterized by the mean geometric spacings L_0 and alignments and by the degree of fluctuation about these means. The average alignment of SAQDs is $\langle 100\rangle$, and we characterize the range of order by, n_{cor}, the number of dots in a row whose positions are

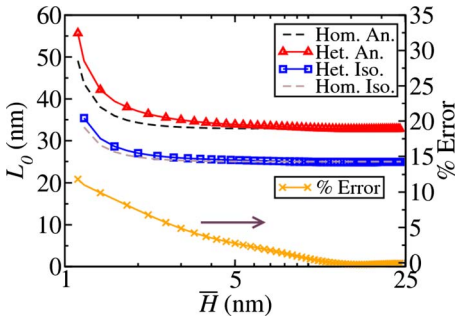

FIG. 6. (Color online) Average dot spacing L_0 as function of $\bar{H}$ for Ge/Si at 600 K from isotropic and anisotropic calculations. Corresponding homogeneous approximations are shown as dashed lines. The percent error in is shown for the anisotropic homogeneous approximation.

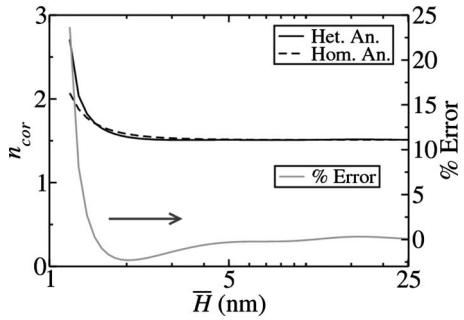

FIG. 7. Number of correlated dots n_{cor} for small height fluctuations Ge/Si at 600 K for anisotropic heterogeneous and anisotropic homogeneous calculations. Also shown, error in n_{cor} from anisotropic homogeneous approximation.

likely to be well correlated, meaning that they are likely to be both regularly spaced and well aligned. In the following discussion, we present calculations for different average film heights, and for each film height we calculate average dot spacing and the number of correlated dots when film height fluctuations reach atomic scale size. For the second part, for finding n_{cor}, we use the film height correlation function and associated correlation lengths which were derived previously.[37,43]

A. Average dot spacing

As done previously,[21,35–37,43] we estimate the average initial spacing between dots to be $L_0=2\pi/k_0$. Figure 6 shows a plot of L_0 against $\bar{H}$ and compares it to the results for the *anisotropic homogeneous* and *isotropic approximations*. The error associated with the homogeneous approximation is also shown. We report values for $\bar{H}=1.2$ nm in Table I. Typically experiments correspond to values of $\bar{H}$ that are less than 20 ML (4.25 nm). For the example studied here (Ge/Si at 600 K), the value of average spacing for *anisotropic heterogeneous* elasticity calculation varies between 32.8 to 55.7 nm.

B. Order analysis using correlation functions

The autocorrelation function and its Fourier transform, also known as the power spectrum, are very useful for characterizing dot order.[37,62,63] The autocorrelation function is defined as

$$C^A(\Delta\mathbf{x}) = \frac{1}{A}\int d^2\mathbf{x}h(\mathbf{x}+\Delta\mathbf{x})h(\mathbf{x}). \tag{11}$$

For an imperfectly periodic array of SAQDs the autocorrelation function decays away from the origin. The distance over which the autocorrelation function decays is known as the correlation length L_{cor}. The value $2L_{cor}$ represents the distance over which the SAQDs appear to be periodic meaning regularly spaced and well aligned.

The power spectrum is

$$C^A_{\mathbf{k}} = |h_{\mathbf{k}}|^2. \tag{12}$$

The power spectrum for a nearly periodic array of SAQDs will have peaks with finite width Δ_k. The spectrum peak width Δ_k is related to the correlation length L_{cor} by $L_{cor}=1/\Delta_k$.

Each simulation or experiment corresponds to one particular realization with its own autocorrelation function; however, for sufficiently large simulation sizes, the fluctuations in $C^A(\Delta\mathbf{x})$ are small, and the ensemble average of the autocorrelation functions can be predicted and provides a good estimate of individual autocorrelation functions and spectrum functions.[37] The ensemble average of the autocorrelation function is the correlation function $C(\Delta\mathbf{x})=\langle C^A(\Delta\mathbf{x})\rangle=\langle h(\Delta\mathbf{x})h(\mathbf{0})\rangle$. Similarly, the ensemble average spectrum function is $C_{\mathbf{k}}=\langle C^A_{\mathbf{k}}\rangle$, where $C_{\mathbf{k}}$ is also the Fourier transform of $C(\Delta\mathbf{x})$ and $C_{\mathbf{k}}$ is the coefficient in the covariance of the Fourier components $h_{\mathbf{k}}$; $\langle h_{\mathbf{k}}h^*_{\mathbf{k}'}\rangle=C_{\mathbf{k}}\delta^2(\mathbf{k}-\mathbf{k}')$, where $\delta^2(\mathbf{k}-\mathbf{k}')$ is the two-dimensional Dirac delta function.

The spectrum function can be solved using Eqs. (7), (9), and (10),[36]

$$C_{\mathbf{k}} \approx \frac{D\Omega k_b T}{(2\pi)^2\sigma_0}k^2 e^{2\sigma_0 t}\sum_{n=1}^{4} e^{-(1/2)L_\parallel^2(k_\parallel k_0)^2-(1/2)L_\perp^2 k_\perp^2}, \tag{13}$$

where $L_\parallel=\sqrt{2\sigma_\parallel t}$ and $L_\perp=\sqrt{2\sigma_\perp t}$ are the correlation lengths. $L_\parallel$ gives about half the length over which the dot spacing is regular, while $L_\perp$ gives about half the length over which a row of dots is straight. Of the two correlation lengths, $L_\perp$ tends to be smaller and thus more limiting. Taking the inverse Fourier transform, the correlation function is

$$C(\Delta\mathbf{x}) \approx \frac{D\Omega k_b T k^2}{\pi\sigma_0 L_\parallel L_\perp}e^{2\sigma_0 t}[e^{-(1/2)(\Delta x^2/L_\parallel^2+\Delta y^2/L_\perp^2)}\cos(k\Delta x) + e^{-(1/2)(\Delta x^2/L_\perp^2+\Delta y^2/L_\parallel^2)}\cos(k\Delta y)]. \tag{14}$$

Figure 7 shows the number of correlated dots calculated as $n_{cor}=2L_\perp/L_0$ for the small fluctuation stage [$C(\Delta\mathbf{x}=\mathbf{0})=1$ ML^2]. Both error and number of correlated dots decline sharply for a small increment in film height above the critical film height. We find the error drops from 24% at $\bar{H}=4.25$ ML to 3% at $\bar{H}=4.95$ ML.

IV. CONCLUSION

Most theoretical and many numerical models of SAQD growth approximate film-substrate systems as elastically homogeneous. We have examined the effect of elastic hetero-

geneity on the SAQD mean spacing estimate and the order estimates developed in Refs. 37 and 36. We have performed a linear analysis incorporating both elastic heterogeneity and elastic anisotropy. We quantify the effect of heterogeneity as percent error in the calculated values of elastic energy density and order estimates based on homogeneous approximation. We show that the homogeneous approximation of the film-substrate system can lead to significant errors in the calculations for formation and ordering of SAQDs. For the case of Ge/Si system at 600 K the upper bound for error in the calculated value of elastic energy density is found to be as large as 26%. For a typical average film height, $\bar{H}=4.25$ ML, we calculate an error of about 11% in the estimation of average spacing between the SAQDs. Using a stochastic model, and the film height correlation functions, we find that the error in the estimated number of correlated dots declines quickly as $\bar{H}$ increases. The error in the estimated number of correlated dots drops from about 24% at $\bar{H}=4.25$ ML to about 3% at $\bar{H}=4.95$ ML. For thinner films, the thin-film approximations can reduce this error, but error still remains as the thin-film approximation actually overestimates the effect of elastic heterogeneity. In general, we find that the most error is due to using the *isotropic* approximation. For the *isotropic heterogeneous* approximation[21] the error in mean dot spacing estimate remains more or less constant at 34% for values of $\bar{H}<20$ ML. We did not report order predictions from isotropic models, as they are inappropriate for order and alignment estimates.[43]

The interplay between elastic strain, surface energy, and surface diffusion can be quite complicated. Errors introduced by the elasticity portion of models can confound our ability to asses how well we model surface and wetting energy. Given the challenge of developing accurate models of surface and wetting energies, it is essential that the elasticity part of the calculation be correct. Inclusion of both elastic heterogeneity and elastic anisotropy represents an important step in the development of a complete nonlinear stochastic model required for a more comprehensive quantitative analysis, for example, incorporating surface energy and diffusive anisotropy.

ACKNOWLEDGMENTS

C.K. gratefully acknowledges the support of The Pennsylvania State University Graduate Fellowship program.

APPENDIX: ELASTIC ENERGY COEFFICIENT

The increase in elastic energy due to the addition of a small material volume at the surface is just the elastic energy density at the surface.[59] We calculate the elastic energy density using perturbation theory following Ref. 37, but here we take elastic heterogeneity into account. This calculation was performed previously but only with the approximation of isotropic elasticity.[22,42] Here we incorporate both elastic heterogeneity and elastic anisotropy to calculate the elastic energy density at the film surface.

We consider a flat film on a substrate. The lattice mismatch between the film and the substrate introduces a misfit strain ϵ_m in the film and leads to a uniform stress distribution in the film given by[37,59]

$$\tilde{\sigma}_m = \begin{bmatrix} \sigma_m & 0 & 0 \\ 0 & \sigma_m & 0 \\ 0 & 0 & 0 \end{bmatrix}, \tag{A1}$$

where $\sigma_m = M\epsilon_m$ and M is the biaxial modulus,

$$M = [c_{11}^f + c_{12}^f - 2(c_{12}^f)^2/c_{11}^f], \tag{A2}$$

where c_{11}^f and c_{12}^f are elastic constants for the film. We perturb the film surface so the film height fluctuates as

$$h(\mathbf{x}) = h_0 e^{ikx}, \tag{A3}$$

where the Cartesian coordinate system is set up so that $z=0$ or the x-y plane lies at the interface of the film-substrate system, and the x-direction is aligned along $\mathbf{k}$. Then, we calculate the elastic energy to first order in the perturbation amplitude h_0. This calculation requires four steps. First we must find the surface normal vector $\mathbf{n}$ to first order in h_0. Then, we must find the admissible equilibrium eigenmodes for the elastic displacement that have the same periodicity as the height perturbation. Then we must find the eigenmode coefficients from the surface boundary conditions and internal matching conditions (compatibility and equilibrium). Finally, we find the elastic energy density at the free surface to first order in h_0. The first step is simple, to the first order in h_0 the normal to the surface of the film is given by

$$\mathbf{n}(\mathbf{x}) = -ikh_0 e^{ikx}\mathbf{e}_x + \mathbf{e}_z. \tag{A4}$$

The remaining three steps follow.

We find the elastic deformation eigenmodes that have the same periodicity as the perturbation, and that satisfy internal equilibrium; working with the displacement field $\mathbf{u}$ automatically satisfies compatibility away from internal interfaces. We first construct the rank 4 elastic stiffness tensor for both film and the substrate for an arbitrary passive rotation $\theta_\mathbf{k}$ of the x-y axes so that $\mathbf{k}$ can lie along any direction in the (001) plane, while Eq. (A3) remains the same.

$$c_{qrst}^{f/s}(\theta_\mathbf{k}) = \sum_{i,j,k,l=1}^{3} R(\theta_\mathbf{k})_{qi} R(\theta_\mathbf{k})_{rj} R(\theta_\mathbf{k})_{sk} R(\theta_\mathbf{k})_{tl} c_{ijkl}^{f/s}, \tag{A5}$$

where we will use the superscript f for the film and s for the the substrate, respectively, and $R(\theta_\mathbf{k})$ is the passive rotation matrix representing the rotation of the x-y axes in the counterclockwise direction by an angle $\theta_\mathbf{k}$ about the z-axis. To match boundary conditions in a later step, displacements must have the form

$$u_l^f(x,y,z) = U_l e^{k(ix+\kappa z)}, \tag{A6}$$

$$u_l^s(x,y,z) = V_l e^{k(ix+\zeta z)}, \tag{A7}$$

where κ and ζ are unknown eigenvalues. Note that in the case of isotropic elasticity, the eigenvalues κ and ζ become degenerate, and one must add additional terms proportional to $ze^{k(ix+\kappa z)}$ and $ze^{k(ix+\zeta z)}$. The stress tensors in the film and the substrate are

$$\sigma_{qr}^{f} = \sum_{s,t=1}^{3} c_{qrst}^{f} \frac{\partial u_s^f}{\partial x_t} + (\tilde{\sigma}_m)_{qr}, \tag{A8}$$

$$\sigma_{qr}^{s} = \sum_{s,t=1}^{3} c_{qrst}^{s} \frac{\partial u_s^s}{\partial x_t}. \tag{A9}$$

For the film, the elastic equilibrium equations are

$$\sum_{q,s,t=1}^{3} \frac{\partial}{\partial x_q} c_{qrst}^{f}(\theta_{\mathbf{k}}) \frac{\partial}{\partial x_s} u_t^f = 0, \quad n = 1 \cdots 3, \tag{A10}$$

$$\left[\sum_{t=1}^{3} C_{rt}^{f}(\theta_{\mathbf{k}}, \kappa) U_t \right] k^2 e^{k(ix+\kappa z)} = 0, \tag{A11}$$

where

$$C_{rt}^{f}(\theta_{\mathbf{k}}, \kappa) = \sum_{q,s=1}^{3} c_{qrst}^{f}(\theta_{\mathbf{k}})(i\delta_{q1} + \delta_{q3}\kappa)(i\delta_{s1} + \delta_{s3}\kappa). \tag{A12}$$

To obtain nontrivial solutions, we set the determinant of $C_{rt}^{f}(\theta_{\mathbf{k}}, \kappa)$ to zero. We thus obtain six eigenvalues of κ denoted by κ^p with $p = \cdots 6$. Each value of $\kappa = \kappa^p$ is substituted back into $C_{rt}(\theta_{\mathbf{k}}, \kappa)$, and Eq. (A11) is solved to find the corresponding eigenvectors U_l^p. The displacement components for the film in terms of the unknown coefficients A_p are thus

$$u_l^f = ih_0 \epsilon_m \sum_{p=1}^{6} A_p U_l^p e^{k(ix+\kappa^p z)}, \tag{A13}$$

where we assume that the perturbing elastic field displacement components are proportional to ϵ_m and h_0, and we put the prefactor $i = \sqrt{-1}$ in for convenience. We use the same procedure to find the eigenvalues and eigenvectors for the substrate displacements u_l^s, where $C_{rt}^{s}(\theta_{\mathbf{k}}, \zeta)$ has the same form as Eq. (A12), but using the substrate elastic constants, c_{qrst}^{s}. Six eigenvalues ζ^p are obtained; however, we assume that the substrate is a semi-infinite solid so the displacement field $u_l^s = 0$ at $z = -\infty$. Thus, we only retain the three eigenvalues with $\mathrm{Re}[\zeta^p] > 0$ that satisfy this condition and discard the other three. We find the displacement components of the substrate,

$$u_l^s = ih_0 \epsilon_m \sum_{p=1}^{3} B_p V_l^p e^{k(ix+\zeta^p z)}, \tag{A14}$$

where V_l^p are the eigenvectors and B_p are the unknown coefficients.

We now find the nine unknown coefficients (A_p and B_p) using the traction-free boundary condition at the surface and the internal matching conditions at the film-substrate interface, namely, equilibrium and compatibility. The traction on the surface of the film is

$$T_r = \sum_{q=1}^{3} \sigma_{qr}^{f} n_q, \tag{A15}$$

where $z = \bar{H} + h(\mathbf{x})$. Substituting Eq. (A8) into Eq. (A15), we get

$$T_r = \sum_{q,s,t=1}^{3} \left[c_{qrst}^{f}(\theta_{\mathbf{k}}) \frac{\partial u_s}{\partial x_t} \right] n_q + (\tilde{\sigma}_m)_{rq} n_q$$
$$= i\epsilon_m h_0 \sum_{q,s,t=1}^{3} \sum_{p=1}^{6} c_{qrst}^{f} k A_p U_s^p (i\delta_{t1} \cdots + \kappa^p \delta_{t3}) e^{k(ix+\kappa^p z)} n_q + (\tilde{\sigma}_m)_{rq} n_q. \tag{A16}$$

Again, we substitute $z = \bar{H} + h(\mathbf{x})$, and we keep only terms up to first order in h_0 to get

$$T_r = \left\{ \sum_{s=1}^{3} \sum_{p=1}^{6} [ic_{3rs1}^{f}(\theta_{\mathbf{k}}) + \kappa^p c_{3rs3}^{f}(\theta_{\mathbf{k}})] A_p \cdots \cdots \times U_s^p e^{k\kappa^p \bar{H}} - M\delta_{r1} \right\} ik\epsilon_m h_0 e^{ikx}. \tag{A17}$$

Since the traction on the film surface must be zero, we have

$$\sum_{s=1}^{3} \sum_{p=1}^{6} [ic_{3rs1}^{f}(\theta_{\mathbf{k}}) + \kappa^p c_{3rs3}^{f}(\theta_{\mathbf{k}})] A_p U_s^p e^{\kappa^p k\bar{H}} = M\delta_{r1}, \tag{A18}$$

giving three equations for $r = 1 \cdots 3$.

The force balance at the internal film-substrate interface requires

$$\sigma_{3r}^{f} = \sigma_{3r}^{s}|_{z=0}. \tag{A19}$$

In terms of the unknown coefficients A_p and B_p, we can write Eq. (A19) as

$$\sum_{s=1}^{3} \sum_{p=1}^{6} (ic_{3rs1}^{f} + \kappa^p c_{3rs3}^{f}) A_p U_s^p = \sum_{s=1}^{3} \sum_{p=1}^{6} (ic_{3rs1}^{s} \cdots + \zeta^p c_{3rs3}^{s}) B_p V_s^p \tag{A20}$$

for $r = 1 \cdots 3$. For the compatibility between the film and the substrate at the interface, the displacements of the film and the substrate must be equal, so that

$$u_q^f = u_q^s|_{z=0}. \tag{A21}$$

In terms of the unknowns, the compatibility equation can be written as

$$\sum_{p=1}^{6} A_p U_i^p = \sum_{q=1}^{3} B_q V_i^q \tag{A22}$$

giving three equations $i = 1 \cdots 3$. We then calculate the nine coefficients $A_p(\theta_{\mathbf{k}}, k\bar{H})$ with $p = 1 \cdots 6$ and $B_q(\theta_{\mathbf{k}}, k\bar{H})$ with $q = 1 \cdots 3$ using using Eqs. (A18), (A20), and (A22).

Following Ref. 37, the we find the elastic energy at the film surface to first order in h_0 to be

$$U = U_0 + M\epsilon_m (\partial_{x_1} u_1^f + \partial_{x_2} u_2^f)|_{z=\bar{H}}, \tag{A23}$$

where U_0 is the elastic energy density of the unperturbed flat film, a constant. Using Eq. (A13)

$$U = U_0 - \mathcal{E}_{\theta_{\mathbf{k}}}(k\bar{H})kh_0 e^{ikx}, \tag{A24}$$

where

$$\mathcal{E}_{\theta_{\mathbf{k}}}(k\bar{H}) = M\epsilon_m^2 \sum_{p=1}^{6} A_p(\theta_{\mathbf{k}}, k\bar{H}) U_1^p(\theta_{\mathbf{k}}) e^{\kappa^p k\bar{H}}, \tag{A25}$$

where we note that A_p will depend on $\theta_{\mathbf{k}}$, k, and $\bar{H}$, and U_l^p will depend on $\theta_{\mathbf{k}}$. By the principle of superposition, we can use the elastic energy coefficient $\mathcal{E}_{\theta_{\mathbf{k}}}(k\bar{H})$ for sums of periodic perturbations as well, so that $U(\mathbf{x}) = U_0 - \int d^2\mathbf{k}\mathcal{E}_{\theta_{\mathbf{k}}}(k\bar{H})kh_{\mathbf{k}}e^{i\mathbf{k}\cdot\mathbf{x}}$.

[1] D. Bimberg, M. Grundmann, and N. N. Ledentsov, *Quantum Dot Heterostructures* (Wiley, West Sussex, 1999).
[2] M. Bayer, O. Stern, P. Hawrylak, S. Fafard, and A. Forchel, Nature (London) **405**, 923 (2000).
[3] T. Akiyama, H. Kuwatsuka, T. Simoyama, Y. Nakata, K. Mukai, M. Sugawara, O. Wada, and H. Ishikawa, IEEE Photonics Technol. Lett. **12**, 1301 (2000).
[4] E. A. Viktorov and P. Mandel, Appl. Phys. Lett. **88**, 201102 (2006).
[5] B. E. Kane, Nature (London) **393**, 133 (1998).
[6] J. M. Elzerman, R. Hanson, L. H. W. van Beveren, B. Witkamp, L. M. K. Vandersypen, and L. P. Kouwenhoven, Nature (London) **430**, 431 (2004).
[7] M. G. Tanner, D. G. Hasko, and D. A. Williams, Microelectron. Eng. **83**, 1818 (2006).
[8] S.-S. Li, J.-B. Xia, Z. L. Yuan, Z. Y. Xu, W. Ge, X. R. Wang, Y. Wang, J. Wang, and L. L. Chang, Phys. Rev. B **54**, 11575 (1996).
[9] S.-S. Li and J.-B. Xia, Phys. Rev. B **55**, 15434 (1997).
[10] O. P. Pchelyakov, Y. B. Bolkhovityanov, A. V. Dvurechenski, L. V. Sokolov, A. I. Nikiforov, A. I. Yakimov, and B. Voigtländer, Semiconductors **34**, 122947 (2000).
[11] M. Grundmann, Physica E (Amsterdam) **5**, 167 (2000).
[12] P. Petroff, A. Lorke, and A. Imamoglu, Phys. Today , 46 (2001).
[13] H.-Y. Liu, B. Xu, Y.-Q. Wei, D. Ding, J.-J. Qian, Q. Han, J.-B. Liang, and Z.-G. Wang, Appl. Phys. Lett. **79**, 2868 (2001).
[14] F. Heinrichsdorff, M. Mao, N. Kirstaedter, A. Krost, D. Bimberg, A. Kosogov, and P. Werner, Appl. Phys. Lett. **71**, 22 (1997).
[15] D. Bimberg, N. Ledentsov, and J. Lott, MRS Bull. **27**, 531 (2002).
[16] M. Friesen, P. Rugheimer, D. E. Savage, M. G. Lagally, D. W. van der Weide, R. Joynt, and M. A. Eriksson, Phys. Rev. B **67**, 121301 (2003).
[17] Y.-C. Cheng, S. Yang, J.-N. Yang, L.-B. Chang, and L.-Z. Hsieh, Opt. Eng. (Bellingham) **42**, 11923 (2003).
[18] R. Krebs, S. Deubert, J. Reithmaier, and A. Forchel, J. Cryst. Growth **251**, 7427 (2003).
[19] H. Sakaki, J. Cryst. Growth **251**, 9 (2003).
[20] B. J. Spencer, P. W. Voorhees, and S. H. Davis, Phys. Rev. Lett. **67**, 3696 (1991).
[21] B. J. Spencer, P. W. Voorhees, and S. H. Davis, J. Appl. Phys. **73**, 4955 (1993).
[22] W. T. Tekalign and B. J. Spencer, J. Appl. Phys. **96**, 5505 (2004).
[23] W. T. Tekalign and B. J. Spencer, J. Appl. Phys. **102**, 073503 (2007).
[24] Y. Obayashi and K. Shintani, J. Appl. Phys. **84**, 3141 (1998).
[25] F. M. Ross, J. Tersoff, and R. M. Tromp, Phys. Rev. Lett. **80**, 984 (1998).
[26] C. S. Ozkan, W. D. Nix, and H. J. Gao, J. Mater. Res. **14**, 3247 (1999).
[27] H. J. Gao and W. D. Nix, Annu. Rev. Mater. Sci. **29**, 173 (1999).
[28] V. Holy, G. Springholz, M. Pinczolits, and G. Bauer, Phys. Rev. Lett. **83**, 356 (1999).
[29] M. Ortiz, E. Repetto, and H. Si, J. Mech. Phys. Solids **47**, 697 (1999).
[30] Y. Zhang, A. Bower, and P. Liu, Thin Solid Films **424**, 9 (2003).
[31] Y. W. Zhang and A. F. Bower, Appl. Phys. Lett. **78**, 2706 (2001).
[32] M. Meixner, R. Kunert, and E. Scholl, Phys. Rev. B **67**, 195301 (2003).
[33] P. Liu, Y. W. Zhang, and C. Lu, Phys. Rev. B **67**, 165414 (2003).
[34] P. Liu, Y. W. Zhang, and C. Lu, Phys. Rev. B **68**, 035402 (2003).
[35] A. A. Golovin, S. H. Davis, and P. W. Voorhees, Phys. Rev. E **68**, 056203 (2003).
[36] L. H. Friedman, J. Electron. Mater. **36**, 1546 (2007).
[37] L. H. Friedman, J. of Nanophotonics **1**, 013513 (2007).
[38] C. Kumar and L. H. Friedman, J. Appl. Phys. **101**, 094903 (2007).
[39] A. Ramasubramaniam and V. B. Shenoy, J. Eng. Mater. Technol. **127**, 434 (2005).
[40] A. Ramasubramaniam and V. B. Shenoy, J. Appl. Phys. **97**, 114312 (2005).
[41] X. Niu, R. Vardavas, R. E. Caflisch, and C. Ratsch, Phys. Rev. B **74**, 193403 (2006).
[42] B. J. Spencer, S. H. Davis, and P. W. Voorhees, Phys. Rev. Lett. **47**, 9760 (1993).
[43] L. H. Friedman, Phys. Rev. B **75**, 193302 (2007).
[44] R. J. Asaro and W. A. Tiller, Metall. Trans. **3**, 1789 (1972).
[45] M. A. Grinfeld, Sov. Phys. Dokl. **31**, 831 (1986).
[46] Y. U. Wang, Y. M. Jin, and A. G. Khachaturyan, Acta Mater. **52**, 81 (2004).
[47] A. Rastelli, M. Stoffel, J. Tersoff, G. S. Kar, and O. G. Schmidt, Phys. Rev. Lett. **95**, 026103 (2005).
[48] A. Rastelli, M. Stoffel, U. Denker, T. Merdzhanova, and O. G. Schmidt, Phys. Status Solidi A **203**, 3506 (2006).
[49] Y. H. Tu and J. Tersoff, Phys. Rev. Lett. **93**, 216101 (2004).
[50] Z. Suo and Z. Zhang, Phys. Rev. B **58**, 5116 (1998).
[51] M. J. Beck, A. van de Walle, and M. Asta, Phys. Rev. B **70**, 205337 (2004).
[52] V. B. Shenoy and L. B. Freund, J. Mech. Phys. Solids **50**, 1817 (2002).
[53] J. Tersoff, B. J. Spencer, A. Rastelli, and H. von Känel, Phys. Rev. Lett. **89**, 196104 (2002).
[54] A. E. Romanov, P. M. Petroff, and J. S. Speck, Appl. Phys. Lett. **74**, 2280 (1999).
[55] Z. M. Zhao, T. S. Yoon, W. Feng, B. Y. Li, J. H. Kim, J. Liu, O. Hulko, Y. H. Xie, H. M. Kim, K. B. Kim *et al.*, Thin Solid Films **508**, 195 (2006).
[56] P. Liu, Y. W. Zhang, and C. Lu, Phys. Rev. B **68**, 195314 (2003).
[57] B. J. Spencer, P. W. Vorhees, and J. Tersoff, Phys. Rev. B **64**, 235318 (2001).
[58] A. A. Golovin, M. S. Levine, T. V. Savina, and S. H. Davis, Phys. Rev. B **70**, 235342 (2004).
[59] L. B. Freund and S. Suresh, *Thin Film Materials: Stress, Defect Formation and Surface Evolution* (Cambridge University Press, Cambridge, 2003), Chap. 8.
[60] L. E. Vorbyev, *Handbook Series On Semiconductor Parameters* (World Scientific, Singapore, 1996), Vol. 1.
[61] M. S. Hegazy and H. E. Elsayed-Ali, J. Appl. Phys. **99**, 054308 (2006).
[62] J. Stangl, T. Roch, V. Holy, M. Pinczolits, G. Springholz, G. Bauer, I. Kegel, T. H. Metzger, J. Zhu, K. Brunner *et al.*, J. Vac. Sci. Technol. B **18**, 2187 (2000).
[63] G. Springholz, M. Pinczolits, V. Holy, S. Zerlauth, I. Vavra, and G. Bauer, Physica E (Amsterdam) **9**, 149 (2001).